Nonpercolative behavior of the magnetic-field-induced local tunneling conductivity of $La_{0.75}Ca_{0.25}MnO_3$/MgO(100) thin films

S. A. Köster,* V. Moshnyaga, B. Damaschke, and K. Samwer
Physikalisches Institut, Universität Göttingen, Friedrich-Hund-Platz 1, 37077 Göttingen, Germany
(Received 11 April 2008; published 18 August 2008)

Overall strain-free $La_{1-x}Ca_xMnO_3$, with $x=1/4$, thin films with two different microscopic growth modes and crystal symmetries were examined by scanning tunneling microscopy and spectroscopy. The films were deposited on MgO(100) substrates and show a variation of the tunneling conductivity depending on the microscopic growth modes of the films. Under the influence of an external magnetic field, a general increase in the tunneling conductivity was found instead of the theoretically predicted domainlike growth of some regions. The colossal magnetoresistance effect seems not to require a percolation behavior.

DOI: 10.1103/PhysRevB.78.052404 PACS number(s): 75.47.Lx, 68.37.Ef, 71.30.+h, 75.47.Gk

The colossal magnetoresistance (CMR) manganites[1–3] are in the focus of basic physics to understand the interplay between spin, charge, lattice, and orbital degrees of freedom.[4–7] The metal insulator transition (MIT), transition temperature (T_{MI}), as well as the magnitude of the CMR are controlled by the doping of the A-site ion in $Ln_{1-x}Ae_xMnO_3$ with the lanthanide ions Ln^{3+}=La, Sm, etc., and alkaline-earth ions Ae^{2+}=Ca, Sr, and Ba. The main influences arise from lattice effects[8,9] such as the mean A-site cation radius,[4] the amount of doping x, and the A-site disorder.[10] Small local strain fields and Jahn-Teller distortions of the MnO_6 octahedra appear. Based on these considerations, electronic inhomogeneities and phase separation have been widely discussed and modeled, e.g., Refs. 11–14, although no final and generally accepted theory could be established yet.

Local probes such as scanning tunneling microscopy (STM) and scanning tunneling spectroscopy (STS) can determine the topographic and local electronic properties simultaneously. Experiments using these techniques[15–19] revealed different results, depending on the samples, which range from an electronically inhomogeneous distribution up to a homogeneous behavior of the specimens. In our work we performed STM and STS measurements at different magnetic fields in the vicinity of the MIT. The T_{MI} can be shifted toward higher temperatures by the application of an external magnetic field while the resistivity is decreased. Hence, measurements of the local properties with respect to applied magnetic fields reveal additional information about the nature of the transition compared with temperature-dependent measurements.

For very local probes, such as STM and STS, changing the magnetic field instead of the temperature has the advantage of having exactly the same area to be examined. According to Dagotto's percolation model with two coexisting phases, a domainlike growth of the metallic phase at the expense of an insulating phase with applied magnetic field would be expected.[20] This behavior should be observed in laterally resolved STS measurements. In our experiments, thin films of $La_{1-x}Ca_xMnO_3$ (LCMO) with $x=1/4$ deposited on MgO(100) were used. The compounds with $x=1/4$ belong to the low-temperature ferromagnetic metallic regime of the phase diagram.[21] Two films of the same composition with different microscopic structures were examined with respect to their bulk properties and microscopic electronic properties at temperatures below, but nearby, the MIT. Both samples showed regions of slightly varying tunneling conductivities. With the application of a magnetic field, all of these regions increase their tunneling conductivity and no domainlike growth was observed.

Thin films of LCMO were deposited by the metal-organic aerosol deposition technique[22,23] on MgO(100) substrates at about 900 °C. The important parameter, which was changed for the different films, was the deposition rate, controlled by the aerosol flux v. A flux of $v_{3D}=0.64$ ml/min results in three-dimensionally (3D) grown films with islands and $v_{LL}=0.125$ ml/min leads to a layer-by-layer (LL) grown film. The two different topographies of these samples are shown in Fig. 1 with a mean-square roughness of 2 nm for the 3D film and 0.2 nm for the LL film. The layers of the LL sample show steps of unit-cell height of about 0.4 nm, determined by different line profiles perpendicular to the step edges. The film thicknesses for both films were about 60 nm, determined by small-angle x-ray scattering (not shown here). The out-of-plane lattice parameters were analyzed by x-ray diffraction to be $d_{3D}=0.3869(5)$ nm and $d_{LL}=0.3872(4)$ nm, which are very close to the bulk value.[24] Together with the results from similar films and high-resolution transmission electron microscopy pictures,[23,25] a macroscopic strain can be excluded for both films. Especially the LL films showed only two to three distorted monolayers directly on the substrate interface, which relax via misfit dislocations. Electron-diffraction patterns from similar samples indicate that the 3D sample has an orthorhombic structure and the LL film has a rhombohedral structure with a tendency toward A-site ordering.[25]

Additionally the films were analyzed by standard four-point probe measurements with the magnetic field applied perpendicular to the sample plane. Both showed a MIT with $T_{MI}=262(1)$ K for the 3D film and $T_{MI}=270(1)$ K for the LL film, and the maximum magnetoresistance $\left[=\frac{R(0)-R(H)}{R(0)}\right]$ was 77(2)% and 79(2)%, respectively. The sharpness of the transition was calculated by the maximum α_{max} of the logarithmic derivative $\alpha=d\ln R/d\ln T$ according to Ref. 17. Remarkably these values differed substantially between $\alpha_{max}=46$ for the LL film and $\alpha_{max}=26$ for the 3D film. In general a tendency to have an increased sharpness in the transition from 3D toward LL films was already reported in Ref. 25.

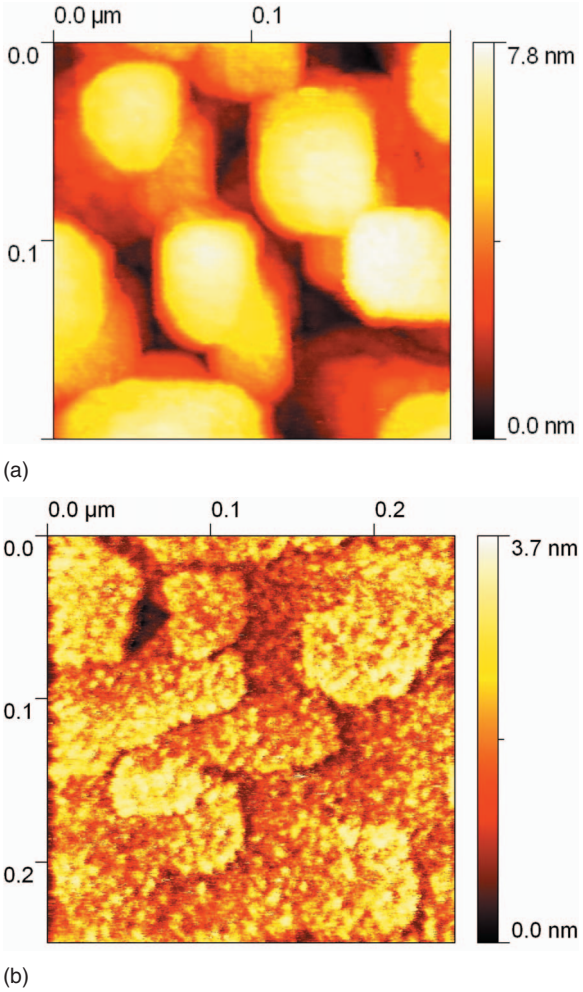

FIG. 1. (Color) (a) Topography of the 3D sample with three-dimensional grainlike growth and a rms roughness of about 2 nm. (b) Topography of LL sample with layer-by-layer growth and a rms roughness of about 0.2 nm. The terraces seen have unit-cell step height.

The STM images were taken under ultrahigh-vacuum conditions with the Cryogenic SFM, a scanning probe microscope from Omicron, equipped with a superconducting magnet, with cut PtIr tips. The magnetic field of $H=40$ kOe was applied perpendicular to the surface of the film. The samples were cleaned in isopropyl alcohol and put onto a heating plate at about 120 °C at ambient pressure prior to mounting to minimize surface contaminations. The topography was always measured in constant current mode. For the spectroscopy, the scanning was stopped during the measurements and the feedback loop was switched off when the current-voltage $[I(U)]$ curve was taken. The linear part around zero bias of each measured $I(U)$ curve was fitted, and the derivative at zero bias was determined and plotted in a two-dimensional map.[16] For an estimation of the quality of the fits, the χ^2 values of the fits were determined to be typically less than 5×10^{-5}.

In Fig. 2 two such STS maps are shown for the 3D film. The images were taken at 258 K at 0.4 V bias and a feedback current of 0.2 nA. The STS maps stem from the same area and showed the same topography. The left map was taken without a magnetic field applied. Regions of different tunneling conductivities can be seen, which are not coupled with the topographical features. The blue and green parts represent lower tunneling conductivities whereas the red and yellow parts have correspondingly higher tunneling conductivities. No sharp interfaces between the regions can be found and the distribution is continuous (Fig. 4). There are individual $I(U)$ curves with very low conductivities down to zero conductivity. However, no contiguous points with clear gaplike features were observed in contrast to highly insulating $Pr_{0.68}Ca_{0.32}MnO_3$ or for $Bi_{0.76}Ca_{0.24}MnO_3$ single crystals.[18] The lateral resolution of the spectroscopy points is ≈2 nm in our case and the resolution of the spectroscopy cannot be much better than ≈80 mV due to the high temperatures. With the application of a magnetic field, the overall conductivity is increased [Fig. 2 (right)] even in the regions with low tunneling conductivity. However, a typical domainlike growth proposed in percolation models[11,13,20] could not be found as a function of external magnetic field.

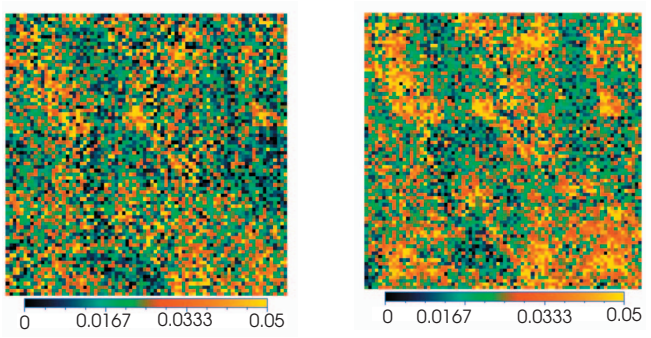

FIG. 2. (Color) STS maps for the 3D sample, taken at 258 K. The size of the images is 200×200 nm with a grid of 80×80 points. The color bars indicate the tunneling conductivities dI/dU at zero bias in nA/V. Left: No magnetic field was applied. Right: A magnetic field of 40 kOe was applied. Both STS maps were taken on exactly the same sample area.

The STS maps for the LL film in Fig. 3, taken at 267 K, 0.4 V bias, and 0.2 nA feedback current, show similar characteristics. Again regions of lower and higher tunneling con-

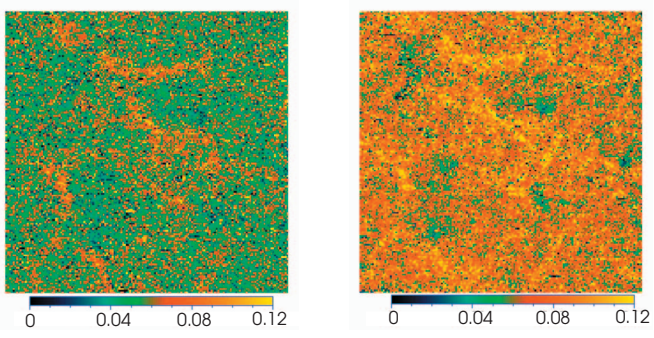

FIG. 3. (Color) STS maps for the LL sample, taken at 267 K. The size of the images is 250×250 nm with a grid of 160×160 spectroscopy points. The color bars indicate the tunneling conductivities dI/dU at zero bias in nA/V. Left: No magnetic field was applied. Right: A magnetic field of 40 kOe was applied. Both STS maps were taken on exactly the same sample area.

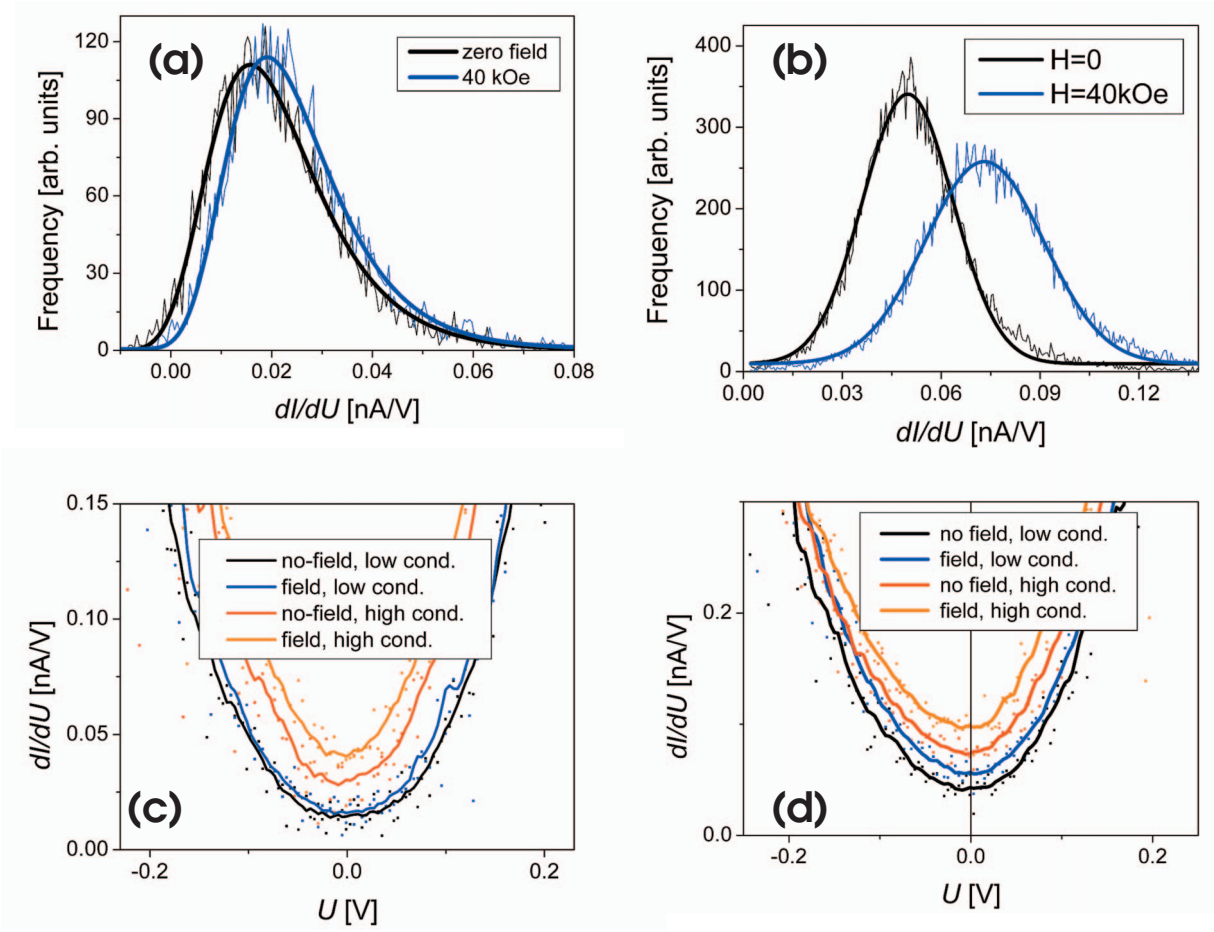

FIG. 4. (Color) Histograms for the 3D and LL measurements shown in Fig. 2 and Fig. 3 in (a) and (b). Black curves represent the nonfield measurement and blue curves the in-field measurements, respectively. Averaged tunneling conductivities around zero voltage $[dI/dU(U=0\ \mathrm{V})]$ of the low conducting and high conducting parts for the STS maps shown above of the 3D sample in (c) and the LL sample in (d).

ductivities coexist but they appear to be smaller than that for the 3D sample, and the distribution is apparently more homogeneous (compare Fig. 2 and Fig. 3). Again the interfaces are not clear. With the application of a magnetic field, the whole STS map changes the color [Fig. 3 (right)] and none of the regions remain with the same tunneling conductivity.

A radial correlation analysis, which is the determination of the smallest self-similar structures in the STS maps, revealed correlation lengths, determined as the radius of the first exponentially fit decay of the radial correlation function, of about $r_{LL} \approx 5-10$ nm for the LL and $r_{3D} \approx 10-17$ nm for the 3D sample, obtained from several measurements. This analysis showed no significant changes with magnetic field.

The distributions of the measured tunneling conductivities are plotted in Figs. 4(a) and 4(b) as histograms for the 3D and LL films shown, respectively. The frequency of the tunneling conductivities with and without field is indicated by the colors black and blue. Distributions consisting of only one maximum can be found. The histogram curves for the LL sample could be fitted exactly by a Gaussian while the histograms for the 3D sample are slightly more asymmetric, which might be due to a somewhat asymmetric distribution of the conductivities; however, the latter is very difficult to separate from noise effects. The histograms are shifted with the application of a magnetic field and the relative shift for the LL films is greater than for the 3D film. The ratio $\Delta\sigma_p = 1 - \frac{\sigma_p(0)}{\sigma_p(40\ \mathrm{kOe})}$ of the peak tunneling conductivities σ_p is 17% for the shown 3D histograms in Fig. 4(a) and 32% for the LL histograms in Fig. 4(b). These observations are representative for all measurements whereas the ratio $\Delta\sigma_p$ changes a little bit.

For measurements with respect to temperature (shown elsewhere[26]), the general picture is similar and, also at lower temperatures, local variations in the tunneling conductivity exist. A general broadening of the histograms with increasing tunneling conductivity can be observed and is attributed mainly to noise effects. The ratio of the width to the peak position stays constant in this case while an increase in the noise relative with the tunneling conductivity is expected in STM measurements. The correlation lengths for lower temperatures stay in the same range, e.g., 4–14 nm, for the LL film.

In Figs. 4(c) and 4(d) the derivatives, determined from $I(U)$ curves averaged over very low conducting and high conducting regions, are shown. The colors black and blue represent the low conducting regions for the nonfield and in-field measurements, respectively, and the red and orange curves stem from the high conducting regions for the non-

field and in-field measurements. First, all regions for the 3D and LL samples show an increase in the tunneling conductivity, namely $dI/dU(U=0\ \mathrm{V})$, in an applied magnetic field. The low conducting regions of the 3D film change less than the higher conducting regions [Fig. 4(c)] but a clear gaplike feature was not seen. For the LL film all regions change their tunneling conductivity by nearly the same value with a field applied.

Besides the comparison of the colored STS maps and the histograms, the above made observations also indicate that there is no domain growth with respect to magnetic-field changes within the films. These "phases," seen on a scale between 4–50 nm, are locally pinned, which do not change their dimension (correlation length) but change their tunneling conductivity. They cannot be compared to those discussed, e.g., by Dagotto *et al.*[11] in terms of percolation, since then domainlike growth and percolation paths would be expected. In our case the regions are locally pinned. Depending on the crystallographic growth, the films with the tendency to a more "ideal" microstructure appear to be more homogeneous in electronic structure, which is also supported elsewhere.[17,27] Probably, the temperature dependence of the conductivity is shifted locally due to these very small inhomogeneities and might lead therefore to the variations in the tunneling conductivity, which are evenly affected by the magnetic field in the MIT region and causing a broadening of the MIT.

Within this discussion of the intrinsic properties of manganites, it has to be noted that STM is a very surface sensitive technique. The electronic and magnetic properties might be changed on the surface due to the symmetry-breaking induced distortion of the oxygen octahedral.[28] To resolve the surface problem, an extended study of the upper surface layers would be required. Unfortunately, there are hardly any studies on LCMO since, even on single crystals, there are no easy cleavage planes. A theoretical study predicts a surface distortion that causes a weakening of the magnetic order at the surface for $La_{0.7}Sr_{0.3}MnO_3$,[29] which could be similar to the LL films here. These surface distortions can be expected to be dependent on the microscopic structure, such as the termination layer, and could therefore be also different for the 3D and LL films, and can contribute to the variations in tunneling conductivity. On the contrary, the general properties, which is the mean tunneling conductivity with respect to the temperature and magnetic field, follow the bulk behavior and therefore they seem not to be fully destroyed in the surface layers detected by the STM. The histograms (in this case not taken from exactly the same area) analyzed at different temperatures are also shifted, and at lower temperatures, the histogram peaks appear at higher tunneling conductivities corresponding to the reduced bulk resistivity at these temperatures.[26]

In conclusion, we observed small local variations in the tunneling conductivity on globally strain-free LCMO films with different microscopic textures. The tunneling conductivity is increased with the application of a magnetic field but no domainlike growth occurs. The typically predicted two-phase behavior with percolation cannot be applied to these samples on the length scales discussed. This accounts to the temperature behavior as well as to the observations with applied magnetic fields for the regime below T_{MI}. As often discussed, the disorder, in terms of local strain fields or defects, may play an important role with respect to electronic inhomogeneities, which can explain the differences between the 3D and LL samples. Compared to other experimental results, e.g., Ref. 18, our experiments give hints about some differences between ferromagnetic metallic manganites and those showing charge ordering with respect to phase forming scenarios. From our results it can be concluded that phase separation with percolation is not a necessary prerequisite for the CMR.

This work was supported by SFB Contract No. 602 TP A2 of the German Research Association and the Leibniz-Program is gratefully acknowledged.

*skoeste@gwdg.de

[1] R. von Helmolt *et al.*, Phys. Rev. Lett. **71**, 2331 (1993).
[2] K. Chahara *et al.*, Appl. Phys. Lett. **63**, 1990 (1999).
[3] M. McCormack *et al.*, Appl. Phys. Lett. **64**, 3045 (1994).
[4] J. M. D. Coey *et al.*, Adv. Phys. **48**, 167 (1999).
[5] M. B. Salamon and M. Jaime, Rev. Mod. Phys. **73**, 583 (2001).
[6] L. P. Gor'kov and V. Z. Kresin, Phys. Rep. **400**, 149 (2004).
[7] Y. Tokura, Rep. Prog. Phys. **69**, 797 (2006).
[8] A. J. Millis, Nature (London) **392**, 147 (1998).
[9] H. Y. Hwang *et al.*, Phys. Rev. Lett. **75**, 914 (1995).
[10] L. M. Rodriguez-Martinez and J. P. Attfield, Phys. Rev. B **54**, R15622 (1996).
[11] E. Dagotto *et al.*, Phys. Rep. **344**, 1 (2001).
[12] M. Uehara *et al.*, Nature (London) **399**, 560 (1999).
[13] K. H. Ahn *et al.*, Nature (London) **428**, 401 (2004).
[14] G. C. Milward *et al.*, Nature (London) **433**, 607 (2005).
[15] M. Fäth *et al.*, Science **285**, 1540 (1999).
[16] T. Becker *et al.*, Phys. Rev. Lett. **89**, 237203 (2002).
[17] J. Mitra *et al.*, Phys. Rev. B **71**, 094426 (2005).
[18] Ch. Renner *et al.*, Nature (London) **416**, 518 (2002).
[19] H. M. Rønnow *et al.*, Nature (London) **440**, 1025 (2006).
[20] M. Mayr *et al.*, Phys. Rev. Lett. **86**, 135 (2001).
[21] P. Schiffer *et al.*, Phys. Rev. Lett. **75**, 3336 (1995).
[22] V. Moshnyaga *et al.*, Appl. Phys. Lett. **74**, 2842 (1999).
[23] V. Moshnyaga *et al.*, Nat. Mater. **2**, 247 (2003).
[24] P. G. Radaelli *et al.*, Phys. Rev. B **56**, 8265 (1997).
[25] V. Moshnyaga *et al.*, Phys. Rev. Lett. **97**, 107205 (2006).
[26] S. A. Köster, Ph.D. thesis, University of Göttingen, 2007.
[27] L. Sudheendra *et al.*, Phys. Rev. B **75**, 172407 (2007).
[28] J. W. Freeland *et al.*, Nat. Mater. **4**, 62 (2005).
[29] J. M. Pruneda *et al.*, Phys. Rev. Lett. **99**, 226101 (2007).